Accepted manuscript of: A. Bekasiewicz, K. Askaripour, M. Wojcikowski, Tuan-Vu Cao, "Design of a Cellular Dual-Band Sticker Antenna for Thickness-Independent 3D-Printed Substrates", 2024 25th International Microwave and Radar Conference (MIKON), doi: 10.23919/MIKON60251.2024.10633960.

Design of a Cellular Dual-Band Sticker Antenna for Thickness-Independent 3D-Printed Substrates

Adrian Bekasiewicz
Faculty of Electronics Telecom. and Informatics
Gdansk University of Technology
Gdansk, Poland
adrian.bekasiewicz@pg.edu.pl

Khadijeh Askaripour
Faculty of Electronics Telecom. and Informatics
Gdansk University of Technology
Gdansk, Poland
khadijeh.askaripour@pg.edu.pl

Marek Wojcikowski
Faculty of Electronics Telecom. and Informatics
Gdansk University of Technology
Gdansk, Poland
marek.wojcikowski@pg.edu.pl

Tuan-Vu Cao
Department of Digital Technologies
Norwegian Institute for Air Research
Oslo, Norway
tvc@nilu.no

***Abstract*—Additive manufacturing technology provides high flexibility in designing custom enclosures for prototype devices such as nodes of distributed sensor networks. Although integration of components is desired from the perspective of sensor mobility, it might negatively affect the performance of radio-connectivity due to couplings between the antenna and system peripherals, as well as other unaccounted effects of the 3D printed enclosure. In this work, a design of a dual-band cellular antenna is considered. The structure is optimized to work on plastic substrates characterized by thicknesses ranging from 1 mm to 5 mm, respectively. The antenna features a –10 dB bandwidth within frequencies from 0.74 GHz to 1.05 GHz and 1.49 GHz to 1.92 GHz. Owing to a simple topology the structure can be implemented in the form of a copper-based sticker and attached on a 3D printed material (e.g., the enclosure of the device). The radiator has been compared against the state-of-the-art antennas in terms of bandwidth and gain.**

Keywords—3D printing, antenna design, numerical optimization, cellular antenna, substrate thickness.

I. Introduction

Development of modern antennas is a challenging task that involves addressing a set of requirements related to field characteristics (e.g., gain, radiation pattern, etc.) [1]-[5] and electrical (e.g., operational bandwidth, reflection, etc.) performance [6]-[10], but also physical constraints (e.g., size, shape, weight, etc.) [11]-[15]. For systems such as distributed sensor networks, the antenna and its transceiver are intended to operate at cellular frequencies to enable uninterrupted transmission of the environmental data for further post-processing on a central server [16]-[18].

The development of antenna structures for cellular networks is a popular research direction [1]-[15]. The design tasks often focus on maintaining planar topology, but also small size, wideband operation, or increased gain. In [19], a dual-band loop radiator dedicated to operate in the frequency ranges around 900 MHz and 1800 MHz has been proposed. The radiator features a small geometry protruded from a relatively large ground plane which makes it applicable to mobile terminals. Another variant of the topology, designed around the inverted *L* geometry with coupling feed, has been considered in [20]. A planar quasi-monopole structure with circular polarization has been proposed in [21]. The antenna offers a low axial ratio over a 0.99 GHz bandwidth of interest. In [22], a tri-band geometry implemented on a multi-layer substrate that covers cellular frequencies but also the range used by global navigation systems has been discussed. Other realizations include dual-band designs dedicated for inkjet-based fabrication on a thin film substrate or antennas integrated onto the enclosure manufactured using additive technology [23], [24].

Regardless of diverse implementations and performance figures, the above mentioned structures have been developed as independent components, which limits their usefulness for operating within larger systems. The reason is that the antenna is a transformer between the guided transmission line and a wireless propagation medium. Consequently, its performance is not only a result of carefully selected (and optimized) topology but also interactions with the environment. The latter might include an enclosure (i.e., housing), and/or connector used for excitation of the radiator, but also other components located in the vicinity of the radiator [16], [25]. Although for mass-market products the effects of the environment are normally accounted for during system integration, the problem is often neglected when the development of prototypes, or experimental devices is considered [16]. Widespread use of additive manufacturing technologies for the development of prototype devices further augments the problem as the large scale of integration—resulting from tightly packed off-the-shelf modules—poses a challenge in terms of ensuring acceptable performance of radio-connectivity gear. From this perspective, the problem concerning design of antennas characterized by increased tolerance to the properties of the nearest environment (dedicated, e.g., for small-scale prototype systems) remains open.

In this work, a dual-band antenna for cellular communication is presented. The structure is optimized to operate on plastic, 3D printed substrates with thickness values ranging from 1 mm to 5 mm, respectively. The proposed structure is characterized by –10 dB reflection within the frequency ranges of at least 0.74 GHz to 1.05 GHz and 1.49 GHz to 1.92 GHz. Owing to simple, single-layer topology, it can be manufactured in the form of an adhesive copper sticker and attached on the 3D printed components such as enclosures of sensor networks. The radiator has been compared against the state-of-the-art antennas from the literature in terms of operational bandwidth and gain.

II. Antenna Structure

Consider a dual-band antenna of Fig. 1. The structure is based on a design of [23]. It integrates two folded dipoles with offset feeds that are mirrored so as to ensure symmetrical radiation response. The driven elements are excited through a 50 Ohm concentric line. The modifications introduced to the antenna include re-design of the geometry using rectangular stubs, introduction of stepped loads, and increased number of design parameters. The proposed changes result in a simplification of the topology and its

This work was supported in part by the National Science Center of Poland Grant 2021/43/B/ST7/01856 and National Center for Research and Development Grant NOR/POLNOR/HAPADS/0049/2019-00.

increased flexibility in terms of applicability to 3D printed materials with various thicknesses. The structure is dedicated to work on a polyethylene terephthalate modified with glycol (PET-G) material which is a popular choice for components manufactured using fused deposition modeling [16]. The permittivity and loss tangent of PET-G are 2.87 and 0.01, respectively [26]. Note that maintaining simple geometry is important as the antenna is to be manufactured using non-standard methods (i.e., other than photolithography). For instance, it can be cut from the adhesive copper sheet (e.g., using a plotter) and then attached to the 3D-printed component (hence the radiator is referred to as a sticker).

The vector of antenna design variables is $\boldsymbol{x} = [l_1\ l_2\ l_3\ l_4\ l_5\ s_1\ s_2\ s_3\ s_4\ w_1\ w_2\ w_3\ w_4\ w_5\ w_6\ w_7]^T$. The constant parameter is $o = 5$, whereas the external dimensions of the structure are $A = l_1 + l_4 + w_6 + w_7$ and $B = s_1 + 2(w_1 + w_2 + s_4)$, respectively. The unit for all parameters is mm. The design ranges for optimization are defined by the following lower and upper bounds $\boldsymbol{l} = [40\ 10\ 10\ 40\ 10\ 10\ 0.5\ 4\ 1\ 1\ 1\ 1\ 2\ 2\ 2\ 2]^T$ and $\boldsymbol{u} = [80\ 50\ 50\ 80\ 50\ 50\ 3\ 10\ 8\ 8\ 8\ 8\ 8\ 8\ 12\ 12]^T$.

The structure EM simulation model is implemented in CST Microwave Studio and evaluated using its time domain solver [27]. The radiator is intended to operate within the $f_{l.1}$ = 0.75 GHz to $f_{h.1}$ = 1 GHz and $f_{l.2}$ = 1.65 GHz to $f_{h.2}$ = 1.9 GHz ranges, respectively. The mentioned bands cover a set of channels dedicated to cellular communication technologies (from the second to the fifth generation). The examples include uplink and downlink frequencies for channels 3, 5, 8, and 27 of the long-term evolution (LTE) standard, but also (among others) the corresponding channels of the 5th generation systems. The structure is dedicated to work on substrates with thicknesses ranging from at least h_1 = 1 mm to h_2 = 5 mm, which is a rather typical choice for custom enclosures of the prototype devices, or other components manufactured using additive technology [16], [28].

III. Optimization Method

A. Problem Formulation

Let $\boldsymbol{R}(\boldsymbol{x}, \boldsymbol{h})$ be the reflection responses of the structure obtained over the discrete frequency sweep $\boldsymbol{f}$ for the vector of input parameters $\boldsymbol{x}$ and the set 3D printed substrates with different $\boldsymbol{h}$. The problem concerning the optimization of the antenna to operate for substrates with diverse thicknesses can be formulated as a follows:

$$\boldsymbol{x}^* = \arg\min_{\boldsymbol{x}\in\boldsymbol{X}} \left(U\left(\boldsymbol{R}(\boldsymbol{x},\boldsymbol{h})\right)\right) \tag{1}$$

where $\boldsymbol{X}$ represents the feasible region of the search space defined by the lower and upper bounds (cf. Section 2), $\boldsymbol{x}^*$ is the optimum design to be found, U denotes a scalar objective function, whereas $\boldsymbol{h} = \{h_k\}$, k = 1, 2, represents the extreme thickness values to be supported by the radiator under development. In practice, the design objective U is evaluated based on two responses obtained from two EM simulations, each for a different h_k.

The objective function is defined as:

$$U = \beta_1 \sum_{k=1}^{2} U_k + \beta_2 \max\left(B - B_t,\ 0\right)^2 \tag{2}$$

where the last component represents penalty coefficient on antenna width with threshold value set to B_t = 50 mm and the electrical performance is specified in the least square sense:

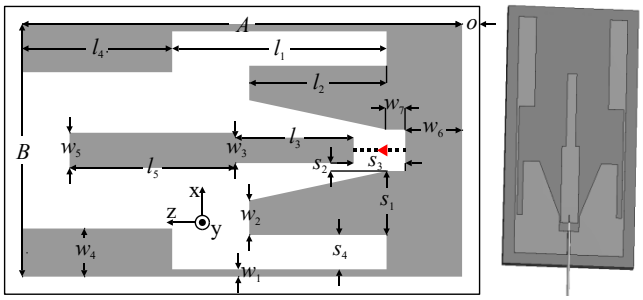

(a) (b)

Fig. 1. A dual-band sticker antenna: (a) geometry with highlight on the design parameters (the arrow indicates location of the concentric feed) and (b) EM model visualization with concentric feed.

$$U_k = \frac{1}{N}\sum_{n=1}^{N} \max\left(R_{k.n} - R_t, 0\right)^2 \tag{3}$$

Here, $R_{k.n} \in \boldsymbol{R}_k = \boldsymbol{R}(\boldsymbol{x}, h_k, \boldsymbol{f}_c)$. The set of frequencies of interest is given as $\boldsymbol{f}_c = \{f_n \in \boldsymbol{f} \mid f_{l.1} \le f_n \le f_{h.1}$ and $f_{l.2} \le f_n \le f_{h.2}\}$. In other words, the function (3) is evaluated over the antenna responses (in decibels) obtained for a discrete set of frequency points within the bands of interest. The threshold value on electrical performance is set to R_t = –13 dB. It is worth noting that the value is lower than the typical –10 dB requirement. It has been set lower so as to provide some margin for errors in the course of the antenna fabrication (e.g., due to tolerances), as well as to maintain acceptable performance even when the thickness of the 3D printed substrate slightly exceeds the assumed 1 mm to 5 mm range. The scaling coefficients are $\beta_1 = \beta_2 = 10^4$ to mitigate the effect of round-up errors on the optimization performance.

B. Design Optimization

Direct solving of (1) is computationally expensive when evaluation of EM simulation models is considered. Instead, the problem can be solved by approximating $\boldsymbol{x}^*$ based on a series of optimizations embedded within a trust-region (TR) framework [29]:

$$\boldsymbol{x}^{(i+1)} = \arg\min_{\left\|\boldsymbol{x}-\boldsymbol{x}^{(i)}\right\|\le\delta} \left(U\left(\boldsymbol{G}^{(i)}(\boldsymbol{x})\right)\right) \tag{4}$$

The minimization of (4) is realized using a standard gradient-based algorithm executed on an iteratively updated linear interpolation model $\boldsymbol{G}^{(i)} = \boldsymbol{R}(\boldsymbol{x}^{(i)}) + \boldsymbol{J}(\boldsymbol{x}^{(i)})(\boldsymbol{x} - \boldsymbol{x}^{(i)})$ [30]. The Jacobian $\boldsymbol{J}$ is generated around $\boldsymbol{x}^{(i)}$ using a large-step finite differences with perturbations determined as a result of a separate optimization embedded within the TR loop [31]. The trust-region radius δ, the update of the model $\boldsymbol{G}$, and termination of the algorithm are governed by a set of standard rules [29]-[31]. Note that separate models $\boldsymbol{G}$ are constructed for extreme thickness values h_k of the substrate (cf. Section III.*A*).

IV. Numerical Results and Comparisons

The initial design for antenna optimization, $\boldsymbol{x}_0$ = [50 25 30 50 30 20 1 7 3 3 3 3 5 5 4 7]^T, has been determined based on the experience-driven adjustment of design parameters. The optimized design, $\boldsymbol{x}^*$ = [50.82 25.11 35.77 42.06 34.06 28.31 0.5 4 2.38 1 7.47 8 8 4.28 10.87 6.99]^T, has been obtained after 16 iterations of the algorithm (4). The computational cost of the antenna tuning amounts to 474 EM simulations (around 21.5 hours of CPU-time using an AMD EPYC 7282 machine with 32 GB of RAM). It should be

reiterated that each evaluation of the objective function involves two EM simulations to account for the effects of substrate thickness changes on the antenna performance (cf. Section III).

Figure 2 shows a comparison of the radiator responses at the initial and optimized designs. The final solution fulfills the defined specification requirements. At the level of –10 dB, the radiator implemented on a 1 mm thick substrate is characterized by bandwidths of 0.35 GHz (38.9%) and 0.65 GHz (35.6%) for lower and upper ranges, whereas for 5 mm 0.37 GHz (44.2%) and 0.49 GHz (27.8%) bandwidths are obtained. It is worth noting that the effects of thickness on the response are much more pronounced for the upper band. A family of antenna responses versus the substrate parameters is given in Fig. 3. The resulting characteristics demonstrate high performance of the radiator even when the material thickness exceeds the ranges considered for optimization. For instance, for the h = 0.5 mm, the antenna only slightly violates the –10 dB threshold within the lower part of the sub-GHz bandwidth. Similarly, for a thickness of h = 9 mm the requirement is violated only for the upper frequencies in the higher band.

Radiation patterns in xy-plane (cf. Fig. 1) at 0.75 GHz, 0.95 GHz, 1.75 GHz, and 1.85 GHz obtained for the extreme substrate thickness values are shown in Fig. 4. The results demonstrate that the antenna features fairly omnidirectional responses regardless of frequency. The change of gain as a function of rotation angle does not exceed 3 dB. A slight degradation of the radiation performance at the ±90° angles is due to the use of symmetrical folded dipole arms (cf. Fig. 1) which reduce the antenna size but also act as obstacles for the radiated field. The maximum gains averaged over the selected frequencies amount to 1.4 dB and 1.33 dB for 1 mm and 5 mm thicknesses, respectively. Hence, a slight degradation of performance with increase of material thickness can be noted. Notwithstanding, the results indicate that the effects of substrate on the radiation responses are relatively low. Overall, the per-frequency discrepancy of maximum gain as a function of h does not exceed 0.5 dB. It is worth noting that the obtained values are merely a by-product of the reflection-based optimization as field-related performance has not been considered at the antenna design stage.

The structure has been compared against the-state-of-the-art antennas from the literature in terms of frequency ranges at the level of –10 dB, bandwidth, and maximum in-band gain [19]-[24]. The radiators considered for comparison include planar geometries, but also a structure dedicated to custom 3D printed enclosures. The results gathered in Table I demonstrate that, for the lower band, the presented structure offers the widest bandwidth and the highest gain (regardless of the selected substrate thickness). For the upper band, the range of operational frequencies also remains competitive. However, the gain is noticeably lower. Again, the effect can be attributed to the topology of the structure. As already indicated, the trapezoidal dipole arms (that correspond to the upper band) are surrounded with the ones that resonate in the lower frequency range which might negatively affect the performance. Furthermore, the topology is not optimized for maximization of radiation performance (the structure was only tuned for electrical parameters). It is worth noting, however, that when compared to benchmark designs, the presented radiator offers a decent responses for a range of substrate material thicknesses. Overall, the results demonstrate the applicability of the presented antenna for use in the cellular connectivity backend with custom enclosures manufactured using 3D printing technology and featuring diversified material thicknesses. Furthermore, the potential to fabrication of the antenna in the form of an adhesive copper film represents an advantage in terms of its integration with prototype devices such as nodes of sensor networks that heavily rely on wireless communication for data exchange.

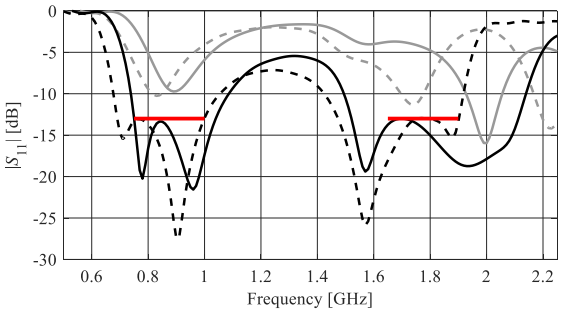

Fig. 2. Reflection of the antenna at the initial (gray) and optimized (black) designs. The responses have been obtained for substrates with h_1 = 1 mm (—) and h_2 = 5 mm (– –), respectively. Red lines denote the bandwidths and reflection levels specified in the objective function of Section III.*A*.

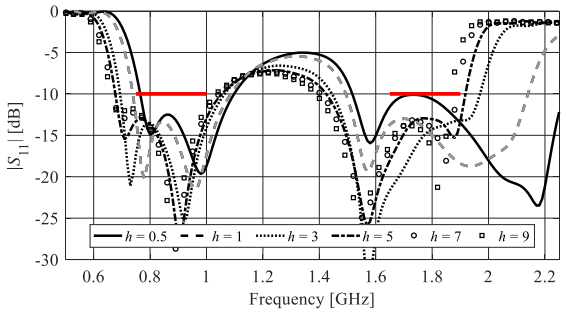

Fig. 3. Reflection responses of the sticker antenna obtained for a range of material thickness values.

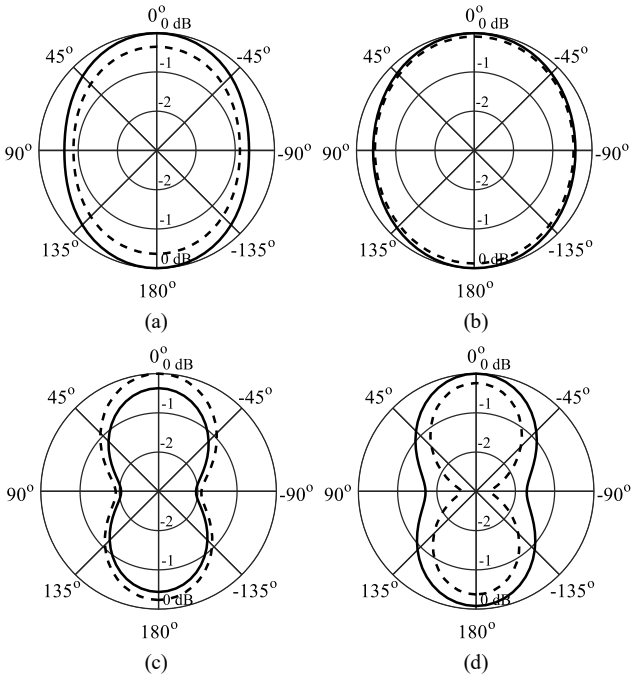

Fig. 4. Normalized radiation patterns (xy-plane; cf. Fig. 1) obtained for the antenna on a substrate with h_1 = 1 mm (—) and h_2 = 5 mm (– –) thickness values at: (a) 0.75 GHz, (b) 0.95 GHz, (c) 1.75 GHz, and (d) 1.85 GHz.

TABLE I. COMPARISON AGAINST THE STATE-OF-THE-ART ANTENNAS

Antenna		Lower band				Upper band			
		f_l [GHz]	f_h [GHz]	BW [GHz]	Gain [dB]	f_l [GHz]	f_h [GHz]	BW [GHz]	Gain [dB]
[24]		0.88	0.97	0.09	1.6	1.36	2.24	0.88	3.2
[20]		0.82	0.96	0.14	1.7	1.70	2.70	1.00	4.3
[23]		0.70	0.95	0.25	1.9	1.9	2.2	0.3	2.3
[19]		0.91	0.99	0.08	0.8	1.73	2.19	0.46	3.3
This work	h_1	0.74	1.09	0.35	2.2	1.49	2.14	0.65	1.0
	h_2	0.68	1.05	0.37	2.1	1.43	1.92	0.49	0.8

V. CONCLUSION

In this work, a dual-band sticker antenna for cellular communication has been presented. The structure has been optimized to work on plastic substrates characterized by diverse thicknesses, which makes it of particular use for custom-based 3D printed enclosures of prototype devices. The antenna is characterized by –10 dB reflection within the frequency ranges from 0.74 GHz to 1.05 GHz and from 1.49 GHz to 1.92 GHz, respectively. Moreover, it offers a fairly omnidirectional radiation pattern in xy-plane with maximum gains of around 2 dB and 1 dB for the lower and upper operational bands. Acceptable electrical performance of the antenna has been demonstrated for PET-G substrate material with thickness values ranging from 0.5 mm to 9 mm which ensures substantial flexibility in terms of its use with a wide range of custom enclosures, e.g., dedicated for nodes of distributed sensor networks.

Future work will involve optimization of the antenna with respect to both the electrical- and field-related performance figures. Furthermore, manufacturing and measurements of the structure prototype upon its implementation on a 3D printed housing of the sensor dedicated to air-quality measurements will also be realized.

REFERENCES

[1] H. Huang, Y. Liu, and S. Gong, "Broadband dual-polarized omnidirectional antenna for 2G/3G/LTE/WiFi applications," *IEEE Ant. Wireless Prop. Lett.*, vol. 15, pp. 576-579, 2016.

[2] W. Song, Z. Weng, Y.-C. Jiao, L. Wang, and H.-W. Yu, "Omni-directional WLAN antenna with common-mode current suppression," *IEEE Trans. Ant. Prop.*, vol. 69, no. 9, pp. 5980-5985, 2021.

[3] X. Yang, Y. Liu and S. -X. Gong, "Design of a wideband omnidirectional antenna with characteristic mode analysis," *IEEE Ant. Wireless Prop. Lett.*, vol. 17, no. 6, pp. 993-997, 2018.

[4] L.H. Ye, Y. Zhang, X.Y. Zhang, and Q. Xue, "Broadband horizontally polarized omnidirectional antenna array for base-station applications," *IEEE Trans. Ant. Prop.*, vol. 67, no. 4, pp. 2792-2797, 2019.

[5] X.-W. Dai, Z.-Y. Wang, C.-H. Liang, X. Chen, and L.-T. Wang, "Multiband and dual-polarized omnidirectional antenna for 2G/3G/LTE application," *IEEE Ant. Wireless Prop. Lett.*, vol. 12, pp. 1492-1495, 2013.

[6] G. Li, H. Zhai, Z. Ma, C. Liang, R. Yu, and S. Liu, "Isolation-improved dual-band MIMO antenna array for LTE/WiMAX mobile terminals," *IEEE Ant. Wireless Prop. Lett.*, vol. 13, pp. 1128-1131, 2014.

[7] Y. Liu, S. Wang, N. Li, J.-B. Wang, and J. Zhao, "A compact dual-band dual-polarized antenna with filtering structures for sub-6 GHz base station applications," *IEEE Ant. Wireless Prop. Lett.*, vol. 17, no. 10, pp. 1764-1768, 2018.

[8] S.J. Yang, W. Duan, Y.Y. Liu, H. Ye, H. Yang and X.Y. Zhang, "Compact dual-band base-station antenna using filtering elements," *IEEE Trans. Ant. Prop.*, vol. 70, no. 8, pp. 7106-7111, 2022.

[9] C. Wang, Y. Chen, and S. Yang, "Dual-band dual-polarized antenna array with flat-top and sharp cutoff radiation patterns for 2G/3G/LTE cellular bands," *IEEE Trans. Ant. Prop.*, vol. 66, no. 11, pp. 5907-5917, 2018.

[10] X.-H. Ding, Q.-H. Zhang, W.-W. Yang, W. Qin, L. Guo, and J.-X. Chen, "A dual-band antenna for LTE/mmWave mobile terminal applications," *IEEE Trans. Ant. Prop.*, vol. 71, no. 3, pp. 2826-2831, 2023.

[11] B. Mun, C. Jung, M.-J. Park, and B. Lee, "A compact frequency-reconfigurable multiband LTE MIMO antenna for laptop applications," *IEEE Ant. Wireless Prop. Lett.*, vol. 13, pp. 1389-1392, 2014

[12] S.W. Lee and Y. Sung, "Compact frequency reconfigurable antenna for LTE/WWAN mobile handset applications," *IEEE Trans. Ant. Prop.*, vol. 63, no. 10, pp. 4572-4577, 2015.

[13] K. Wang, R.A.M. Mauermayer, and T.F. Eibert, "Contour-integrated dual-band compact antenna elements and arrays for low-profile mobile terminals," *IEEE Trans. Ant. Prop.*, vol. 63, no. 7, pp. 3305-3311, 2015.

[14] A. Ramachandran, S. Mathew, V. Rajan, and V. Kesavath, "A compact triband quad-element MIMO antenna using SRR ring for high isolation," *IEEE Ant. Wireless Prop. Lett.*, vol. 16, pp. 1409-1412, 2017.

[15] Q. Zhang and Y. Gao, "A compact broadband dual-polarized antenna array for base stations," *IEEE Ant. Wireless Prop. Lett.*, vol. 17, no. 6, pp. 1073-1076, 2018.

[16] M. Wojcikowski, B. Pankiewicz, A. Bekasiewicz, T.-V. Cao, J.-M. Lepioufle, I. Vallejo, R. Odegard, and H.P. Ha, "A surrogate-assisted measurement correction method for accurate and low-cost monitoring of particulate matter pollutants," *Measurement*, vol. 200, art. no. 111601, 2022.

[17] L.R. Crilley, M. Shaw, R. Pound, L.J. Kramer, et al., „Evaluation of a low-cost optical particle counter (Alphasense OPC-N2) for ambient air monitoring," *Atmos. Meas. Tech*., vol. 11, pp. 709-720, 2018.

[18] A. Di Antonio, O.A.M. Popoola, B. Ouyang, J. Saffell, and R.L. Jones, „Developing a relative humidity correction for low-cost sensors measuring ambient particulate matter," *Sensors*, vol. 18, art. no. 2790, 2018.

[19] Y.-W. Chi and K.-L. Wong, "Quarter-wavelength printed loop antenna with an internal printed matching circuit for GSM/DCS/PCS/UMTS operation in the mobile phone," *IEEE Trans. Ant. Prop.*, vol. 57, no. 9, pp. 2541-2547, 2009.

[20] Y. Hong, J. Tak, Y. Jin, and J. Choi, "A compact planar multi-band antenna with coupling feed for LTE/GSM/UMTS operations," *Int. Symp. Ant. Prop. Conf.*, pp. 501-502, Kaohsiung, Taiwan, 2014.

[21] K. Nadali, P. McEvoy, and M.J. Ammann, "A broadband circularly polarised slot antenna for ambient RF energy harvesting applications," *Int. Workshop Ant. Techn.*, pp. 153-156, Dublin, Ireland, 2022.

[22] S.-T. Fang and J.-W. Sheen, "A planar triple-band antenna for GSM/DCS/GPS operations," *IEEE Ant. Prop. Soc. Int. Symp.*, vol. 2, pp. 136-139, Boston, MA, 2001.

[23] Y. Suzuki and M. Sumi, "Multiband film antenna comprising offset fed dipole elements using inkjet printer for M2M applications," *Int. Workshop Ant. Techn.*, pp. 51-54, Cocoa Beach, FL, 2016.

[24] S. Zhen and A. Shamim, "A 3D printed dual GSM band near isotropic on-package antenna," *IEEE Int. Symp. Ant. Prop.*, pp. 1251-1252, San Diego, CA, 2017.

[25] A. Bekasiewicz and S. Koziel, "Low-cost design optimization of antennas with peripheral components," *Baltic URSI Symp.*, pp. 146-149, Warsaw, Poland, 2020.

[26] J. Zechmeister and J. Lacik, "Complex relative permittivity measurement of selected 3D-printed materials up to 10 GHz," *Conf. Microwave Techn.*, pp. 1-4, Pardubice, Czech Republic, 2019.

[27] CST Microwave Studio, ver. 2018, Dassault Systems, 10 rue Marcel Dassault, CS 40501, Vélizy-Villacoublay Cedex, France, 2018.

[28] C. Bathory, Z. Dobo, A. Garami, A. Palotas, and P. Toth, "Low-cost monitoring of atmospheric PM—development and testing," *J. Environ. Manage*., vol. 304, art no. 114158, 2022.

[29] A. Conn, N.I.M. Gould, P.L. Toint, *Trust-region methods*, MPS-SIAM Series on Optimization, Philadelphia, 2000.

[30] S. Koziel and A. Pietrenko-Dabrowska, "Reduced-cost electromagnetic-driven optimization of antenna structures by means of trust-region gradient-search with sparse Jacobian updates," *IET Microwaves Ant. Prop.*, vol. 13, no. 10, pp. 1646-1652, 2019.

[31] A. Bekasiewicz, "Optimization of the hardware layer for IoT systems using a trust-region method with adaptive forward finite differences," *IEEE IoT J.*, vol. 10, no. 11, pp. 9498-9512, 2023.